

# RSC Advances



This is an *Accepted Manuscript*, which has been through the Royal Society of Chemistry peer review process and has been accepted for publication.

*Accepted Manuscripts* are published online shortly after acceptance, before technical editing, formatting and proof reading. Using this free service, authors can make their results available to the community, in citable form, before we publish the edited article. This *Accepted Manuscript* will be replaced by the edited, formatted and paginated article as soon as this is available.

You can find more information about *Accepted Manuscripts* in the [Information for Authors](#).

Please note that technical editing may introduce minor changes to the text and/or graphics, which may alter content. The journal's standard [Terms & Conditions](#) and the [Ethical guidelines](#) still apply. In no event shall the Royal Society of Chemistry be held responsible for any errors or omissions in this *Accepted Manuscript* or any consequences arising from the use of any information it contains.



Cite this: DOI: 10.1039/c0xx00000x

www.rsc.org/xxxxxx

ARTICLE TYPE

## Structure and growth mechanism of self-assembled monolayers of metal protoporphyrins and octacarboxylphthalocyanine on silicon dioxide

Virginie Gadenne,<sup>\*a,b</sup> Louis Porte<sup>a</sup> and Lionel Patrone<sup>\*a,b</sup>

<sup>a</sup>Aix Marseille Université, CNRS, Université de Toulon, IM2NP UMR

5 7334, 13397, Marseille, France

<sup>b</sup>ISEN-Toulon, IM2NP UMR 7334, Place G. Pompidou, 83000 Toulon, France

Received (in XXX, XXX) Xth XXXXXXXXX 20XX, Accepted Xth XXXXXXXXX 20XX

DOI: 10.1039/b000000x

In this work, we studied the structure and the growth of various conjugated macrocycles SAMs (two  
10 protoporphyrins ZnPP and FePP, and one phthalocyanine ZnPc(COOH)<sub>8</sub>) on silicon oxide previously  
functionalized by aminopropyltrimethoxysilane (APTMS) for covalent grafting of macrocycles on the  
surface. The samples were characterized by atomic force microscopy (AFM), ellipsometry, contact angle  
measurements, Fourier transform infrared (FTIR) and UV-visible spectroscopy.

A growth model of macrocycle layers within three steps was established from ellipsometry and UV-  
15 Visible results at various deposition times. Firstly, a fast adsorption of macrocycles occurs on the surface  
in a disordered way followed by a rearrangement phase. Then, the layers get denser by adsorption of  
supplementary macrocycles on the surface.

Spectroscopic and morphological analyses reveal a specific structure for each deposited macrocycle. The  
size of macrocycle core and the metallic atom nature are shown to be key factors which govern  
20 orientation and assembly of macromolecules on the surface. At last, the essential issue of film stability at  
ambient atmosphere has been addressed.

### Introduction

The design of thin films of conjugated macrocycles such as  
25 porphyrins and phthalocyanines is of great interest due to their  
important potential roles in functional organic materials and  
devices, such as catalysts (1; 2; 3), gas sensors (4; 5; 6; 7),  
transistors (8), or photovoltaic cells (9; 10).

30 Among the several molecular devices described in the literature,  
one can quote the work of Bocian's group on molecular memories  
based on porphyrins as the information storage medium (11; 12;  
13; 14; 15). In their approach, they have used the discrete redox  
states of porphyrins attached to an electroactive surface for  
35 capacitive memory cells.

Other studies show that the optical and electrical properties of  
conjugated macrocycle thin films are extremely sensitive to  
adsorption of gas molecules (NO<sub>2</sub>, SO<sub>2</sub>, and CO<sub>2</sub>), making them  
40 promising candidates for gas sensor applications (16; 17; 18; 19;  
20; 21)

Among various strategies for the formation of macrocycle films  
required for the design of these molecular devices, the leading

45 advantage of self-assembly method is the covalent bonding  
between the molecules and the surface, which replaces weak van  
der Waals or hydrogen bonding as in the case of Langmuir-  
Blodgett films. Therefore self-assembled thin films offer very  
good chemical and physical stability.

50 In the literature, two approaches have been developed for the  
formation of conjugated macrocycle films by self-assembly.  
The first one is the immobilization of the macrocycle flat on the  
surface by covalent bonding between the axial ligand and the  
surface docking sites (22; 23; 24).

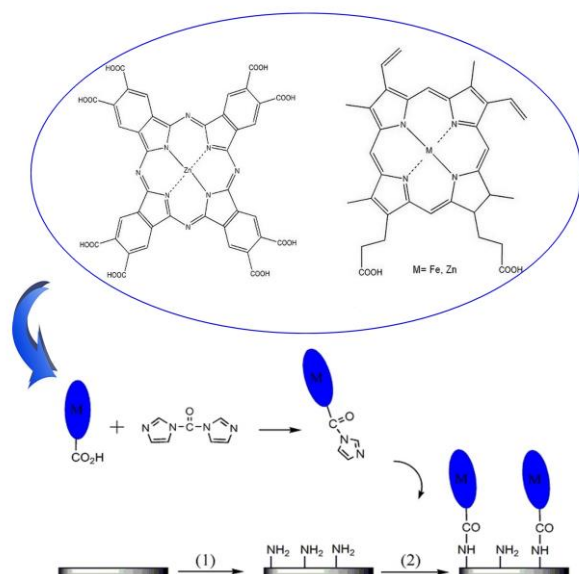


**Fig. 1** Scheme of macrocycle layer formation: 1) Functionalization of SiO<sub>2</sub> surface by APTMS SAM; 2) Covalent grafting of macrocycles on the surface.

This method enables a good control of face-to-face macrocycle arrangement, but the subsequent increase of coordinance degree of the metallic atom of the macrocycles modifies their physico-chemistry properties and limits the possibilities of metallic site exploitation particularly in gas sensor applications.

The second way is the use of functional groups on the macrocycle periphery for the grafting on the surface. This method requires specific macrocycle engineering and synthesis. A lot of studies account for synthesis procedures of porphyrins and their self-assembly on gold surface (25; 26; 27), but so far not much attention has been paid to the structure of porphyrin monolayers. However, the electronic properties of macrocycle layers are closely related to their arrangement on the surface.

Therefore, it is important to study the formation and to characterize the arrangement of porphyrin and phthalocyanine layer on the surface to control their thin film preparation in an ordered way to give rise to the desired physical properties.

That is the motivation of this work firstly devoted to the understanding of the mechanism of molecular thin film formation from a solution for various conjugated macrocycles, secondly both to determine molecular arrangement within the films and to evaluate layer stability at room conditions.

The macrocycle layers were assembled on silicon dioxide (SiO<sub>2</sub>) surface pre-functionalized by amino groups from a solution as depicted in figure 1.

Silicon covered with its native oxide was chosen as substrate since it is suitable both for potential applications and for the formation of robust SAM using tri-functionalized aminosilane molecules as a sticking layer. For the latter, widely used aminopropyltrimethoxysilane (APTMS) self-assembled monolayer (SAM) was prepared at the SiO<sub>2</sub> surface, making it possible to anchor the macrocycle on the surface via an amide

bonding formed between the macrocycle peripheral carboxylic acid moieties activated by a coupling reagent (carboxydiimidazole, CDI), and the amino reactive groups of the APTMS SAM. Such a two-step grafting method has the advantage to be versatile since it is independent from nature of the substrate.

Commercially available zinc and iron protoporphyrin (ZnPP and FePP) and zinc octacarboxylphthalocyanine (ZnPc(COOH)<sub>8</sub>, specially synthesized) were selected due to the carboxylic acid moieties (COOH) substituted in peripheral position. Moreover, due to their amphiphilic nature, these macrocycles are good candidates for the formation of self-assembled monolayers. Note that in addition to large  $\pi$ -stacking interaction both molecules can interact through hydrogen bonding between their peripheral carboxylic acid moieties. This effect should be strongly enhanced in the case of ZnPc(COOH)<sub>8</sub> compared to that of ZnPP due to the presence of eight COOH peripheral groups against only two for the latter.

For the zinc and iron protoporphyrins, the comparison of results obtained by ellipsometry, atomic force microscopy (AFM), UV-visible and infrared spectroscopy could inform us about the impact of the metallic atom nature on the monolayer self-assembly.

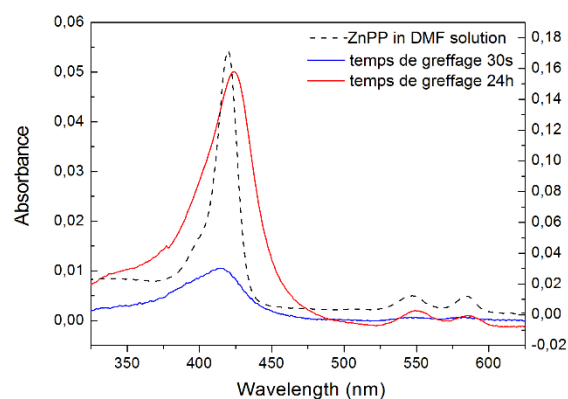
In the same way, comparing the results obtained from the analyses of zinc octacarboxylphthalocyanine SAM with those of zinc protoporphyrin SAM allowed us to clarify the influence of the  $\pi$  conjugated system size on the order of the SAM.

## Results and discussion

### Growth mechanism of macrocycle layers

The growth of macrocycle layers was monitored by ellipsometry and UV-visible spectroscopy measurements on macrocycle films prepared with different deposition durations.

The UV-Visible spectra of macrocycle SAMs for various grafting times and in DMF solution are presented in figure 2.



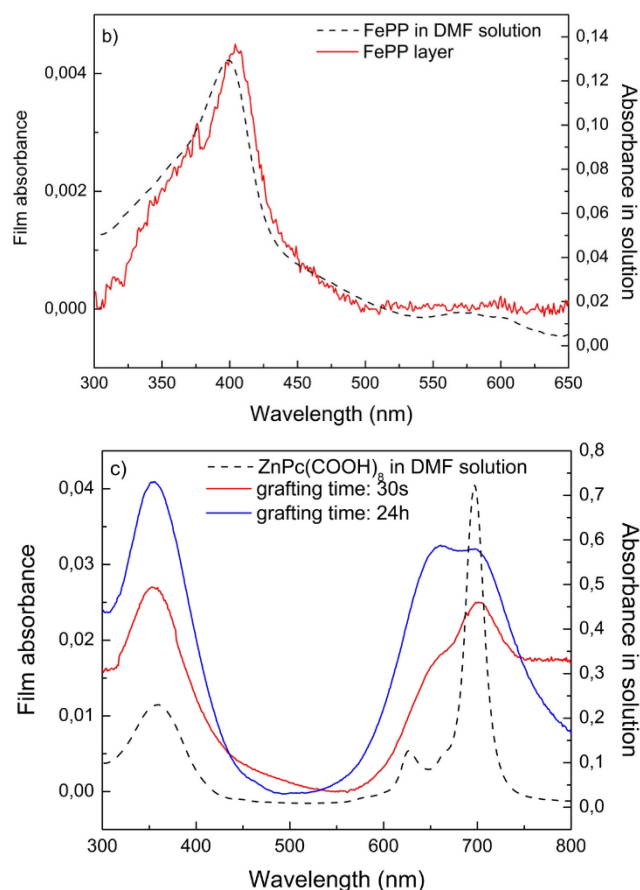


**Fig. 2** UV-Visible absorption spectra of ZnPP (a), FePP(b) and ZnPc(COOH)<sub>8</sub> (c) SAMs and in DMF solution

Information on the aggregation and orientation of the macrocycles on the surface was obtained by comparing UV-Visible spectra measured from film and from solution. Moreover, for all macrocycle SAMs, the characteristic absorption bands were detected which enabled us to definitely identify the macrocycle on the surface.

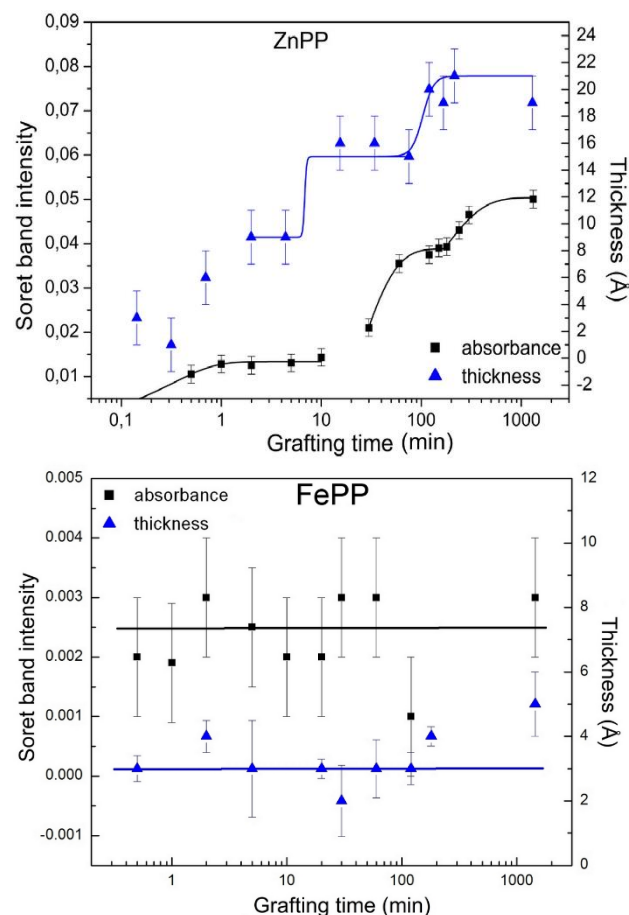
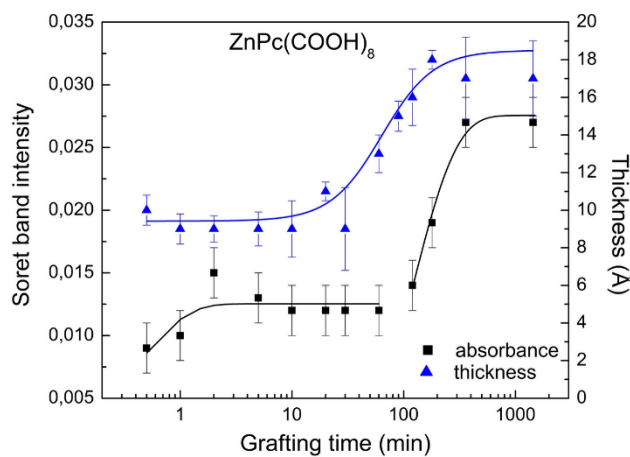


**Fig. 3** Time evolution of thickness and UV-Visible absorption measured at different steps of the growth of each macrocycle film.

In figure 3, for each macrocycle the time evolution of thickness and Soret band intensity is plotted in a logarithm time-scale in order to visualize the short time values.

These two curves show a good correlation between the ellipsometry and UV-Visible measurements. Nevertheless, the time constants were extracted from absorption data because UV-Visible method appeared more sensitive than ellipsometry to macrocycle SAM growth.

The growth kinetics of ZnPc(COOH)<sub>8</sub> and ZnPP SAMs exhibit successive adsorption steps (two for ZnPc(COOH)<sub>8</sub> and three for ZnPP). Each step is best-fitted by the following Langmuir growth function:

$$A = A_{i\max} [1 - b_i \exp^{-t/t_i}], \quad i = 1, 2, 3 \quad \text{eq (1)}$$

Time constants  $t_i$  and step final absorbance  $A_{i\max}$  for the SAMs of ZnPc(COOH)<sub>8</sub> and ZnPP are summarized in table 1.

**Table 1:** Time constants obtained from fit by eq (1) of the growth kinetics of the SAM of ZnPP and ZnPc(COOH)<sub>8</sub>

	$t_1$ (s)	$A_{1\max}$	$t_2$ (min)	$A_{2\max}$	$t_3$ (min)	$A_{3\max}$
ZnPc(COOH) <sub>8</sub>	25±12	0.0125	107±54	0.0275	-	-
ZnPP	19±9	0.0133	19±7	0.0388	150±87	0.0503

For both zinc macrocycles, layer growth begins with a quick



adsorption of molecules on the surface characterized by a first time constant of about twenty seconds. This first adsorption step corresponds to a thickness of macrocycle layers of 9 Å and 10 Å for ZnPP and ZnPc(COOH)<sub>8</sub>, respectively. These values are lower than the theoretical length of molecules which suggests the formation of disordered layers.

Just following this first step (after 30s of grafting time), the UV-visible spectra of ZnPP layers are not very different from that in solution. This translates the lack of order in the layers.

Indeed, as observed for dissolved ZnPP in DMF solution, the UV-visible spectrum of ZnPP layers (figure 2a) exhibits three bands at 417, 547, and 585 nm, assignable to the Soret band and two Q bands respectively. The Soret band is broader due to the chemisorption of ZnPP on silicon oxide surface.

As for ZnPc(COOH)<sub>8</sub>, the UV-visible spectrum in solution (figure 2c) shows a sharp Q-Band at 697 nm indicative of monomeric phthalocyanine, whereas on the SAM, this band is splitted in two peaks: one at 699 nm related to monomer species and the second at 633 nm ascribed to dimers and higher order aggregates (28; 29). After 30s of grafting time, the intensity of the band at 699 nm is still more intense than that of the second band at 633 nm. Thus ordered domains have begun to form but the layers are mostly composed of unpacked areas.

After the first adsorption step, a latency phase followed by a quick increase in the number of adsorbed molecules is observed with a second time constant of 19 and 107 min for ZnPP and ZnPc(COOH)<sub>8</sub> respectively.

For ZnPc(COOH)<sub>8</sub>, after the second adsorption phase the growth of layer reaches a final plateau after five hours of deposition. The final layer thickness is about 19 Å that is near to the theoretical length of molecule (23 Å). The surface density of ZnPc(COOH)<sub>8</sub> calculated from the absorption band at 355 nm (see eq 3) is about  $4.2 \times 10^{-7} \text{ mmol.cm}^{-2}$  which is characteristics of a perpendicular orientation of macrocycles on the surface (30).

During the grafting, the increase in the intensity of the band at 633 nm (figure 2c) can be linked to a densification of the ZnPc(COOH)<sub>8</sub> layers.

Moreover, according to Kasha's molecular exciton theory the splitting of the absorbance band is attributed to the herringbone arrangement of phthalocyanine rings in the SAM. This behavior is usually observed for phthalocyanine films obtained by Langmuir-Blodgett deposition or by evaporation (29).

Conversely, for ZnPP SAM, there are two additional growth steps. The second step of layer growth characterized by a second time constant ( $t_2 \approx 19 \text{ min}$ ) is faster than that of the ZnPc(COOH)<sub>8</sub>. This can be explained by the presence of alkyl chains which could facilitate the rearrangement of macrocycles within the disordered layers.

After this growth phase, a layer thickness of 15 Å is obtained corresponding to a single ZnPP monolayer (31).

The last growth phase ( $t_3 \approx 150 \text{ min}$ ) can be attributed to the formation of a second monolayer by head-to-tail insertion of additional macrocycles into the first one. This head to tail

arrangement of two aromatic moieties seems to be the most stable possible conformation because it maximizes the stacking interactions between the porphyrin cores (32).

Indeed, on the final ZnPP layer, the Soret band is red-shifted from 417 nm to 424 nm and according to the excitonic coupling theory of the electronic transitions in the porphyrin  $\pi$ -system developed by Kasha, the red-shift of the Soret band is consistent with a head-to-tail arrangement of porphyrin  $\pi$ -system. This result indicates that ZnPP molecules form J-aggregates in the SAM. Moreover, from the UV-visible analysis, the estimated surface density of ZnPP is about  $1.8 \times 10^{-7} \text{ mmol.cm}^{-2}$ , and a similar value was found for a densely packed tetrapyrridylporphine monolayer on silicon surface (30).

Contrary to ZnPP, Soret band intensity and thickness of FePP SAM do not change with deposition time (figure 3). With a mean thickness of 3 Å, FePP SAM is quickly formed on the surface, within less than 30 seconds of deposition. The FePP surface density is about  $3.8 \times 10^{-9} \text{ mmol.cm}^{-2}$ , i.e., much lower than for ZnPP. This low surface density together with the low thickness suggests a flat orientation of FePP on the surface, possibly resulting from interactions between amine groups and iron atoms of the protoporphyrins.

Moreover, in the UV-visible spectrum (figure 2b), the Soret band of FePP film is red-shifted towards 405 nm compared to the molecules in solution (398 nm). According to the literature, this absorption band is a feature of pentacoordinate complex formed by interaction between Fe atoms and electro-donor groups like amine moieties. On the other hand, it is also possible that the formation of this complex is due to attachment to the metallic atoms in axial position of diimidazole groups arising from CDI-activated carboxylic groups.

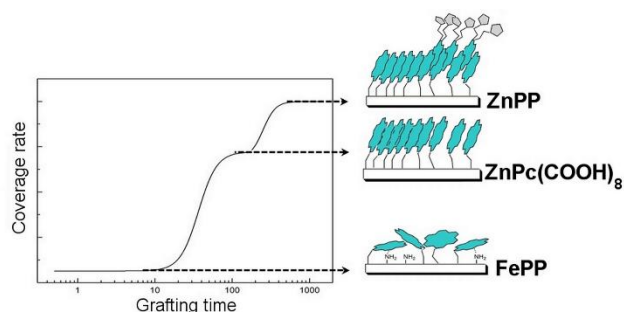


**Fig. 4** Schematic growth curve with the final monolayer arrangement for each macrocycle studied.

In summary, these results enable us to propose a mechanism of conjugated macrocycle growth on the silicon surface in three steps. In the first step, the macrocycles are quickly adsorbed and form a disordered phase on the surface. This leads to strongly hinder the adsorption of additional macrocycles within a first stationary state. This latency phase is accompanied by a rearrangement of macrocycles on the surface.

During such a rearrangement phase, new anchoring sites are available which results in a rapid growth leading to a well-ordered monolayer. Only ZnPP layer keeps growing towards a second final

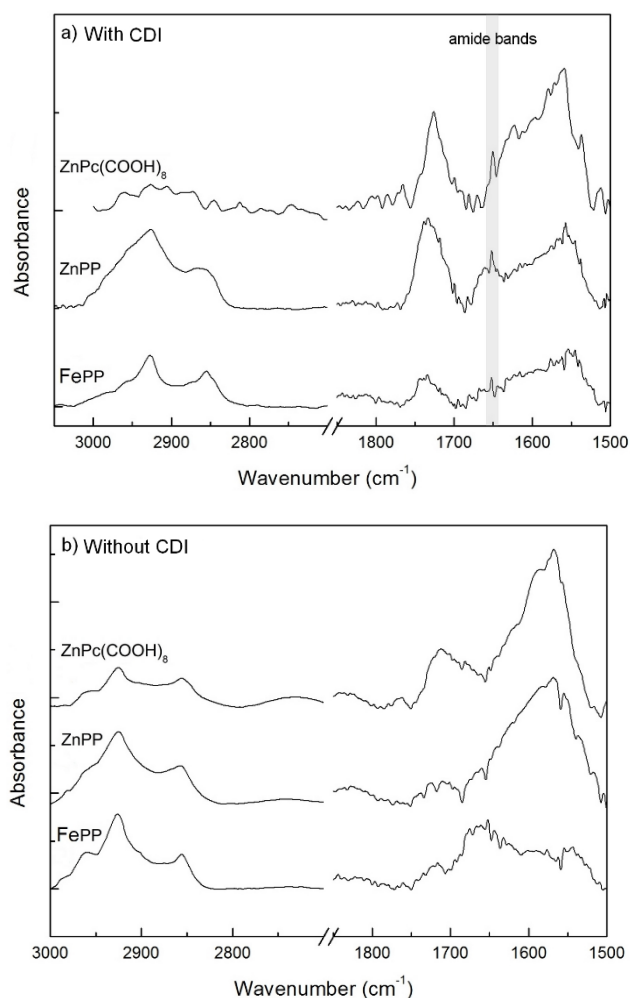
plateau by head-to-tail insertion of molecules into the first layer. In addition, the rapid growth of FePP layer is locked to the first step because the interactions between the iron atom in the porphyrinic cycles and the surface make it impossible the rearrangement phase.

Figure 4 presents a schematic growth curve with the final monolayer arrangement proposed for each macrocycle studied.

### Spectroscopic and morphological analyses of macrocycles layers

In order to obtain complementary information on the final thin film structure, macrocycle layers were also analyzed by ATR-FTIR spectroscopy to identify chemical functional groups and bonding between macrocycles and the surface.

For highlighting the interactions between macrocycles and the surface, ATR-FTIR spectra (figure 5) were achieved on the final macrocycle layers deposited with (a) and without (b) CDI-coupling reagent on the SiO<sub>2</sub> surface functionalized by amino-groups.



**Fig. 5** ATR-FTIR spectra measured on ZnPP, FePP and ZnPc(COOH)<sub>8</sub> SAMs deposited with (a) and without (b) coupling reagent (CDI) on SiO<sub>2</sub> functionalized by amino-groups.

In all infrared spectra, we observe two peaks at 2856 cm<sup>-1</sup> and at 2925 cm<sup>-1</sup> corresponding respectively to the symmetric and antisymmetric stretching modes of CH<sub>2</sub> groups of the alkyl chains

composing the aminosilane underlayer and the protoporphyrin molecule for FePP and ZnPP.

Macrocycle grafting process on the amino-SiO<sub>2</sub> surface drastically modifies ATR-FTIR spectra in the frequency range 1800-1500 cm<sup>-1</sup>.

Without catalyst, a weak band at 1710 cm<sup>-1</sup> is observed resulting from the hydrogen bonded C=O stretching mode of COOH. This band is more intense in ZnPc(COOH)<sub>8</sub> spectra due to the numerous carboxyl groups of this molecule. When the macrocycle is activated by CDI, this band is shifted toward high frequency (1735 cm<sup>-1</sup>). This corresponds to C=O stretching mode of imidazol ester group arising from the activation of carboxylic groups unreacted with the surface amino groups. Furthermore, we can distinguish only for the SAMs prepared with CDI a weak band around 1650 cm<sup>-1</sup> attributable to vibrational mode of amide groups. This band allows confirming the covalent grafting of macrocycles to the APTMS-functionalized SiO<sub>2</sub> surface.

Around 1550 cm<sup>-1</sup>, we find the peak characteristic of porphyrinic skeletal stretch vibrations (33). Without coupling reagent, this band is broader due to the overlap with the band arising from C=O stretching vibration of carboxylate salts.

On the other hand, the spectrum of FePP without CDI exhibits a wide band at 1635 cm<sup>-1</sup>. This band is specific of FePP and more particularly of the iron atom because it is not observed in ZnPP spectrum. According to Slater's study (34), an intense IR absorbance around 1664 cm<sup>-1</sup> suggests the presence of a unident coordination with iron of a carboxylate group coming from a propionate side chain of another FePP. This result suggests that FePP aggregation is built up via an iron-carboxylate linkage between adjacent FePP macrocycles.

Macrocycle layer morphology was also characterized by AFM in tapping mode. The images before and after macrocycle deposition are presented in figure 6.

The weak roughness of FePP layers compared to that of ZnPP may indicate a difference in the arrangement of macrocycles on the surface.

Applying the same process without CDI coupling reagent resulted for the protoporphyrin layers in an increase of roughness and in disordered layers with adsorbed aggregates (images shown in supporting information) favoured by hydrogen interactions between the carboxylic groups of neighbouring macrocycles.

On the contrary, ZnPc(COOH)<sub>8</sub> layers seem better ordered without CDI coupling reagent. This can be explained by hydrogen interactions between macrocycles favouring a compact arrangement that may be hindered by imidazol ester group produced by CDI-activation.

In summary, the use of CDI coupling reagent enable covalent grafting of the macrocycles on the surface by amide bond formation and limits the multilayers build up.



Cite this: DOI: 10.1039/c0xx00000x

www.rsc.org/xxxxxx

ARTICLE TYPE

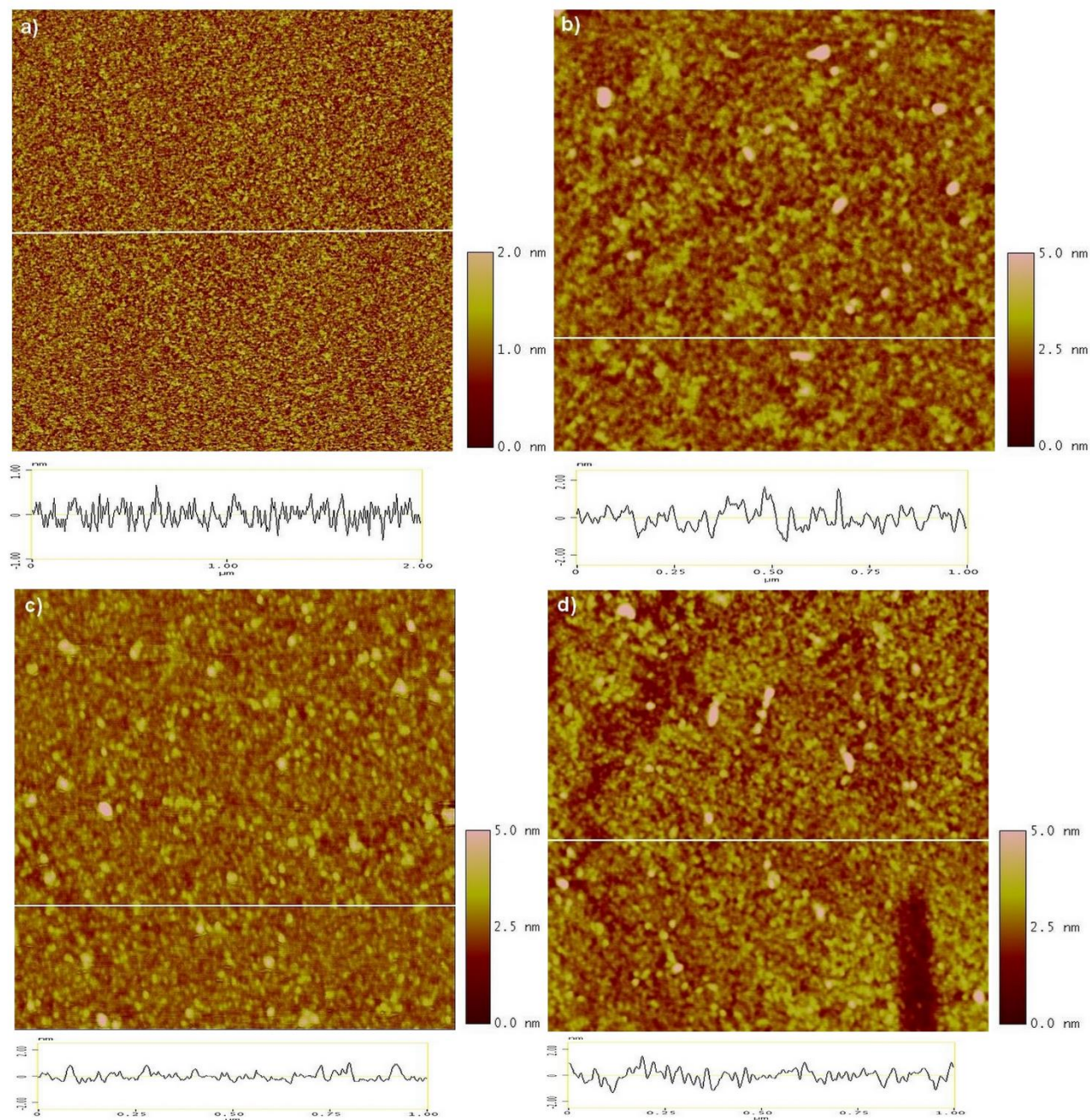


**Fig 6** AFM images ( $1 \times 1 \mu\text{m}^2$ ) of silicon dioxide functionalized by APTMS (a), ZnPP (b), FePP (c) and ZnPc(COOH)<sub>8</sub> (d) adlayers. Typical cross-section are also shown. The image of APTMS monolayer reveals a very smooth surface with roughness of 0.25 nm. After immobilization of macrocycles, the surface morphology is altered with the appearance of small islands on the surface and an increase in roughness to 0.54 nm, 0.42 nm and 0.33 nm for ZnPP, ZnPc(COOH)<sub>8</sub>, FePP layers respectively.



### Stability of the macrocycle layer

As a key point for potential applications of these macrocycle layers at ambient conditions, their time stability has been followed by UV-visible absorption spectroscopy. Evolution of the Soret band intensities for ZnPP and ZnPc(COOH)<sub>8</sub> layers according to storage duration is plotted in figure 7 .

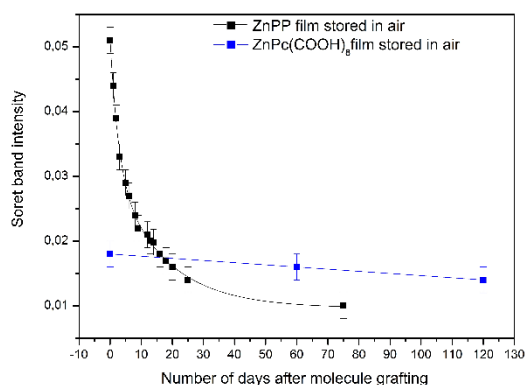


**Fig. 7** Variation of Soret band intensity of the macrocycles films versus the storage duration at room conditions and under argon with a very low amount of oxygen (less than 0.1 ppm).

At room conditions, the Soret band intensity of ZnPP layer strongly decreases during the first day of storage. This decrease could be approximated by the following exponential decay law for the absorbance:

$$\text{Abs} = A (e^{-t/t_1} + e^{-t/t_2}) + B \quad (\text{eq } 2)$$

With  $t_1 = 2.6$  days,  $t_2 = 16.5$  days,  $A = 0.02$  and  $B = 0.01$

When ZnPP film is stored under argon atmosphere (not shown) with a very low oxygen amount (less than 0.1 ppm), this decrease is not observed. So in presence of oxygen, the electronic features of ZnPP layer are altered. The same results are reported by Hirano *et al* (35).

After cyclic voltammetric measurements, they observed an irreversible oxidation of ZnPP film leading to a disappearance of absorption bands. This was attributed to formation of dioxoporphomethene.

On the contrary, the Soret band intensity of the ZnPc(COOH)<sub>8</sub> layers is relatively constant under room conditions.

As a result, the films of ZnPc(COOH)<sub>8</sub> are more stable than those of ZnPP in ambient conditions, which makes them better candidates for applications in molecular devices.

### Conclusion

In conclusion, we have shown that the self-assembly on silicon dioxide surface prefunctionalized by amino groups is a suitable method for the formation of protoporphyrin or carboxylated phthalocyanine layer. Using a CDI coupling reagent promotes the formation of robust amide covalent bonding on the peripheral position allowing the macrocycles standing possibly upright at the

surface.

Combining ellipsometry measurement and UV-visible absorption spectroscopy of conjugated macrocycle layers allowed a model of film growth in three steps to be determined: first the formation of a disordered phase on the surface, followed by a rearrangement process allowing chemisorption of supplementary macrocycles, and at last the achievement of a dense monolayer.

However we also observed that the nature of the metallic atom of protoporphyrins modifies the molecule orientation on the surface. FePP is lying flat on the surface contrary to ZnPP which is oriented perpendicular to the surface with head-to-tail aggregation. Another arrangement type was observed for ZnPc(COOH)<sub>8</sub> film which forms herringbone structure.

On the other hand, a key result is that the phthalocyanine film is more stable at room conditions than protoporphyrin layer. This together with the morphology and the formation characteristics of these macrocycle layers obtained from this work constitute an important step forward to enable their future applications within molecular devices.

### Acknowledgements

The authors are indebted to Mireille Mossoyan-Deneux and Mabinty Bayo-Bangoura for the synthesis of ZnPc(COOH)<sub>8</sub> molecule. The Ministère de l'Enseignement Supérieur et de la Recherche (MESR), Aix-Marseille University, ANR program (ANR-05-NANO-001-05) and « Solutions Communicantes Sécurisées » (SCS) competitive cluster are also acknowledged for financial support. This work could be carried out thanks to equipment mainly funded by the « Objectif 2 » program of the European Economic Community, the FEDER, the « Conseil Général du Var » Council, the PACA Regional Council, Toulon Provence Méditerranée and ISEN-Toulon which are acknowledged.

### Experimental

#### Molecules

The coupling agent aminopropyltrimethoxysilane (APTMS) was obtained from Acros Organics.

Zinc and iron protoporphyrin were purchased from Frontier Scientific and Strem Chemicals respectively and used without further purification.

The octacarboxylphthalocyanine was synthesized according to the procedure described elsewhere (36).

#### Deposition protocol

Before film preparation, the silicon substrate is degreased in a sonicated chloroform bath, and then dried under a nitrogen flow. It is cleaned in a freshly prepared piranha solution (H<sub>2</sub>SO<sub>4</sub>: H<sub>2</sub>O<sub>2</sub>, 7:3 in volume) at 120°C for 30 min and then rinsed abundantly with deionized water and quickly immersed into a beaker of deionized water. After being carefully dried under a nitrogen flow, the

cleaned silicon dioxide surface is quickly immersed into a dilute solution of APTMS in methanol (1% volume) for 24 h at room temperature to prepare the APTMS SAM. The sample is rinsed in a sonicated methanol solution to remove physisorbed molecules of APTMS and immediately immersed into a solution of conjugated macrocycles at 0.1 mM in DMF, with an excess of carboxydiimidazole (CDI) coupling reagent.

Carboxydiimidazole reagent is widely used to activate the reactivity of carboxylic acid groups and enables to form an amide bond between the conjugated macrocycle and amino groups present at the surface. Grafting tests were also performed without this reagent.

After the grafting reaction of macrocycles, the sample is rinsed successively in DMF and ethanol solution and dried under a nitrogen flow before being characterized.

For the growth study of macrocycle layer, the totality of APTMS samples was simultaneously elaborated in the same cleaning bath and the same silanization solution, in order to restrict the reproducibility problem of APTMS layer formation. Each APTMS SAM was then immersed in macrocycle solution during the targeted deposition time, carefully rinsed, dried, and subsequently analysed.

## Characterization

A Sentech SE400 ellipsometer with 632.8 nm He-Ne laser at an incidence angle of 70° allowed us to determine the thickness of molecular layers, using refractive indexes  $n=3.875-0.016i$  for silicon substrate,  $n=1.46$  for silicon oxide and  $n=1.5$  for organic film (APTMS and macrocycles) (37). Reported results are an average of at least 10 measurements at different locations on the substrate.

Measurements of UV-visible absorption spectra were carried out in transmission with a Perkin Elmer Lambda 850 spectrophotometer. For these measurements, macrocycles and the coupling agent were grafted on double side polished ( $rms < 4\text{\AA}$ ) fused silica substrates.

According to Kasha's molecular exciton theory, the position of UV-visible absorption band gives information on the chromophore arrangement on the surface (38).

Moreover, the order of magnitude of macrocycle surface coverage can be deduced from the Beer-Lambert expression (39):

$$d_{\text{surf}} = A/2\epsilon[\text{mmol}\cdot\text{cm}^{-2}] \quad (\text{eq } 3)$$

With  $\epsilon_{\text{ZnPP}} = 13.4 \times 10^5 \text{ cm}^2\cdot\text{mol}^{-1}$ ;  $\epsilon_{\text{ZnPc}(\text{COOH})_2} = 3.2 \times 10^5 \text{ cm}^2\cdot\text{mol}^{-1}$ ;  $\epsilon_{\text{FePP}} = 5.3 \times 10^5 \text{ cm}^2\cdot\text{mol}^{-1}$ .

For each molecule, the extinction coefficient was determined from UV-visible absorption spectra of macrocycles in DMF solutions with different concentrations.

The nature of interactions between each macrocycle and amino groups present on the surface was identified using FTIR spectroscopy in attenuated total reflexion mode (ATR-FTIR). These experiments were performed using a Perkin Elmer Spectrum GX spectrometer equipped with a liquid nitrogen cooled MCT

detector. Molecular SAMs were directly deposited on a trapezoidal silicon crystal allowing the infrared beam to be reflected 25 times in order to improve the absorption signal of molecular layers. All spectra were registered at a resolution of  $4 \text{ cm}^{-1}$ , and 1024 scans were accumulated.

Morphological features of molecular layers were investigated by atomic force microscopy (AFM) measurements in tapping mode (AFM tips with resonance frequency of 150-350 kHz) with Multimode equipment and a Nanoscope IIIa controller from Bruker.

## References

- Ozoemena, K. I. et al *Electrochim. Acta.*, 2006, **51**, 2669.
- Armijo, F., et al. *J. Mol. Catal. A: Chem.*, 2007, **268**, 148.
- Halma, M., et al. *J. Mol. Catal. A: Chem.*, 2003, **243**, 44.
- Ashkenasy, G., et al. *Acc. Chem. Res.*, 2002, **35**, 121.
- Pilloud, D. L., et al. *Langmuir*, 1998, **14**, 4809.
- Royer, J. E., et al. *Langmuir*, 2012, **28**, 6192.
- Simmendinger, W., et al. *Sens. Actuators, B.*, 2013, **19**, 54.
- Xiao, K., et al. *J. Phys. Chem. B* 2003, **107**, 92269.
- Karthikeyan, S. et al. *J. Phys. Chem.*, 2013, **117**, 10973.
- Liang, F., et al. *Sol. Energy Mater. Sol.*, 2010, **94**, 1803.
- Roth, K. M., et al. *J. Am. Chem. Soc.*, 2003, **125**, 505.
- Roth, K. M., et al. *J. Phys. Chem. B*, 2002, **106**, 8639.
- Thamyongkit, P., et al. *J. Org. Chem.*, 2006, **71**, 1156.
- Roth, K. M et al *Langmuir*, 2002, **18**, 4030.
- Gryko, D. T., et al. *J. Org. Chem.*, 2000, **65**, 7345.
- Chen, Y., et al. *Sens. Actuators, B.*, 2011, **155**, 165.
- Dedigama, A., et al. *J. Phys. Chem. C*, 2012, **116**, 826.
- Gulino, A., et al. *Chem. Mater.*, 2005, **17**, 521.
- Ma, M et al. *J. Phys. Chem. B*, 2006, **110**, 14911.
- Min, M et al. *J. Phys. Chem. C*, 2007, **111**, 8649.
- Yang, Y-Y et al. *J. Electroanal. Chem.*, 2013, **688**, 379.
- Cruz, F. D. et al. *Thin Solid Films*, 1999, **349**, 155.
- Li, X. et al. *Thin Solid Films*, 2004, **457**, 372.
- Miao, P. et al. *J. Phys. Chem. B*, 2000, **104**, 1285.
- Gryko, D. T. et al. *J. Org. Chem.*, 1999, **64**, 8635.
- Gryko, D. T. et al. *J. Org. Chem.*, 2000, **65**, 7356.
- Clausen, C., et al. *J. Org. Chem.*, 2000, **65**, 7363.
- Maggioni, G. et al. *Sens. Actuators, B*, 2007, **127**, 150.
- Kai, L. et al. *Chem. Phys. Lett.*, 2007, **438**, 36.
- Li, D.Q. et al. *J. Am. Chem. Soc.*, 1993, **115**, 6975.
- Li, C. et al. *Langmuir*, 2003, **19**, 779.
- Scolaro, L. M. et al. *J. Phys. Chem. B*, 2002, **106**, 2453.
- Gaffo, L. et al. *J. Mater. Sci.*, 2010, **45**, 1366.
- Slater, A. F. G. et al. *Proc. Natl. Acad. Sci.*, 1991, **88**, 325.
- Hirano, C. et al. *J. Colloid Interface Sci.*, 2004, **280**, 478.
- Gadenne, V. et al. *J. Colloid Interface Sci.*, 2011, **359**, 47.
- Li, Z. et al. *Langmuir*, 2001, **17**, 4887.
- Kasha, M. et al *Pure Appl. Chem*, 1965, **11**, 371.
- DeQuan, L. et al *Chem. Mater.*, 1994, **6**, 803.
- Clausen, C., et al. *J. Org. Chem.*, 2000, **65**, 7371.